RESETTABLE LANDING GEAR FOR MARS HOPPER

William S. Gullotta[(1)], **Coleton G. Kirchner**[(2)], **Aaron P. Yuengert**[(3)], **Peter A. Zink**[(4)]

[(1)] *Boston University College of Engineering, 110 Cummington Mall, Boston, MA, USA 02215, wgullott@bu.edu*
[(2)] *Boston University College of Engineering, 110 Cummington Mall, Boston, MA, USA 02215, kirchner@bu.edu*
[(3)] *Boston University College of Engineering, 110 Cummington Mall, Boston, MA, USA 02215, yuengert@bu.edu*
[(4)] *Boston University College of Engineering, 730 Commonwealth Ave, Boston, MA, USA 02215, pzink@bu.edu*

1 ABSTRACT

[In this research,] a passive electromagnetic shock absorption solution was developed for a repeated landing Mars Hopper by taking into account the rigid requirements for operation on Mars and the dynamic landing forces upon the vehicle. Mathematical models were derived for the landing dynamics and the electromagnetic damper, computer simulations and analysis on the landing gear were performed, and a physical prototype to test the damper was constructed. It was found that the electromagnetic damper landing gear is a predictable, reliable, and extremely effectual solution for resettable landing gear for the Mars hopper or any future interplanetary repeated landing vehicles. The steps required to implement the landing gear include the development of the mathematical models, refined design of the components to withstand operation on Mars, and the creation and testing of a scale physical model of the entire hopper.

2 INTRODUCTION

2.1 Background

The University of Leicester Space Research Centre has proposed a new type of Mars lander to replace the NASA rovers that are currently in use on the planet. The vehicle they have proposed uses a radioisotope powered CO_2 rocket to perform ballistic "hops" of up to 1 km at a time, as shown in Figure 1. This "Mars Hopper" has a longer range,and can traverse more difficult terrain than any previous mission to Mars' surface.

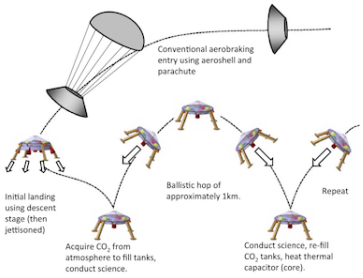

Figure 1: Mars Hopper Mission Profile[1]

However, the Hopper faces one developmental problem: there are no viable designs for resettable legs for interplanetary landers in existence. All previous legged landers have been design to facilitate a single touchdown, using a non-reusable crushable honeycomb material in the legs to attenuate the impact. The legs were then either left behind, as is the case in the Apollo missions, or the lander remained permanently stationary, as in the Phoenix mission.

2.2 Problem Definition

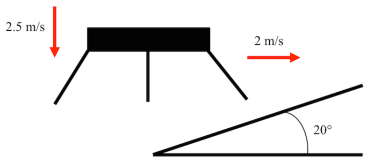

Figure 2: Landing Scenario

The design of the landing gear for a repeated landing Mars probe must achieve several mandatory requirements. The most important of these is that the shock absorption system must be resettable as the craft is expected to make at least 200 hops. Secondly, the landing gear configuration must support a dynamic load of 1000 kg at a maximum vertical velocity of 2.5 m/s and a maximum horizontal velocity of 2 m/s. Thirdly, the Mars hopper must be able to land on an inclined slope of 20 degrees with a 2 degree tilt variation[1]. This landing scenario can be seen in Figure 2. Lastly, the system must withstand the vacuum of space. This means that the landing gear cannot use hydraulics. It will also have to resist launch, spaceflight and entry vibrations as well as fluctuations in temperature and pressure.

3 CONCEPT SELECTION

After analyzing the scope of the problem and the time constraints of the project it was quickly realized that the entirety of the landing gear design could not be completed. It was then decided to focus on the aspects of the design specific to the attenuation of the impact forces, namely the generation of the damping force and the resetting of the shock absorber.

3.1 Damping Method

The first function explored was generation of the damping force. The most common reversible shock absorber types are pneumatic and hydraulic. Hydraulic systems were specifically prohibited by our customer as they are unable to perform in space and were omitted from the initial concept selection process. Pneumatics, compressible fluids, and non-Newtonian fluids were then eliminated for several reasons. First, their damping characteristics would change dramatically throughout the Martian day due to the extreme temperature fluctuations on Mars, and second, they would be pressurized and would need to be heavily sealed to travel through the vacuum of space. Active magnetic systems require a power input, and due to the strict power consumption requirements of spacecraft, were eliminated. It was therefore chosen to design a passive electromagnetic system.

3.2 Alternatives Considered

Upon selecting an electromagnetic solution it was found that three possible types of linear magnetic machines exist: synchronous, induction, and permanent magnet [3]. Both synchronous and induction type machines, which typically generate their magnetic fields using powered coils, were rejected because they require an external power supply, while permanent magnet type machines are completely passive. Synchronous type machines also operate at constant speed, making them unsuitable for damping applications.

Figure 3: Tubular Permanent Magnet Configurations[3]

Figure 3 shows the three possible configurations for a permanent magnet damper. In all cases it contains a mover mounted on a shaft which translates through a tubular stator. The first configuration shown is the moving coil. The stator houses the permanent magnets and the mover contains the coils. For the moving coil configuration to work a set of brushes must be added to extract the electricity generated on the mover. The next configuration is the moving iron, which places both the coils and the permanent magnets on the stator. The mover contains an iron core which as it passes through the coils and magnets changes the flux linkage between the two. The final configuration is the moving magnet. This configuration places a permanent magnet and iron core on the mover and the coils on the stator tube. This configuration was selected because it requires no brushes and achieves a higher force density than the moving iron configuration[3].

3.3 Resetting Method

The resetting function was then approached. Pneumatics, linear drives, and magnetic reset options were eliminated due to their complexity. Gravity was eliminated because the force it provides is not strong enough to oppose the damping force. The spring was therefore the simplest and most effective solution and was selected to be developed in the design.

4 MATHEMATICAL MODELING OF TOUCHDOWN DYNAMICS

To determine the parameters of the damping system, the forces on the legs needed to be understood. Mathematical models were developed to calculate the dynamic forces upon the legs upon touchdown.

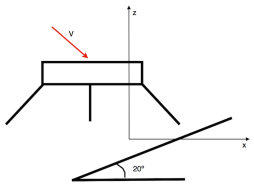

Figure 4: Worst Case Landing Scenario

Based on the problem requirements, the worst-case landing scenario would be a landing at 2.5 m/s in the vertical (z) direction and 2 m/s in the horizontal (x) direction onto a slope of 20° from the horizontal, with the craft oriented such that the primary struts of two legs lie in the x-z plane. Thus, the leading leg would absorb the initial impact all by itself before the other legs touched down. The best-case scenario would be a symmetrical landing on a completely horizontal surface with no horizontal velocity.

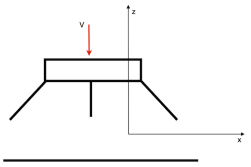

Figure 5: Best Case Landing Scenario

A discrete mathematical model of the best-case scenario was developed as a starting point for understanding the dynamics of the hopper. The best method to model the landing is by using energy and work to determine the equations of motion. The equations of motion can then be used to find the velocity that the damper will move, which determines its physical characteristics. In dynamics this energy method is known as the Lagrangian approach.

4.1 Energy, Work, and Generalized Forces

For these models, each of the legs were assumed to consist of three members, or struts, consisting of a spring-damper system with the entire mass concentrated at the center of the hopper as seen in Figure 6.

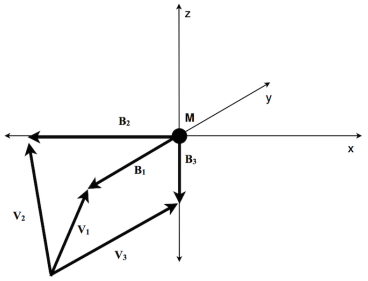

Figure 6: Simplified Hopper Leg Geometry

Where M is the center of mass of the hopper, B_1, B_2, and B_3 are the vectors from the center of mass to where the struts connect, and V_1, V_2, and V_3 are vectors representing the struts.

The kinetic energy of the system is defined as:

$$T^* = \frac{1}{2}mv^2 \tag{1}$$

where m is the total mass of the hopper and v its velocity. The potential energy of the system is defined as:

$$V = mgh + \frac{1}{2}k_p^2 s_p^2 + k_s s_s^2 \tag{2}$$

where g is the gravitational constant, h is the vertical distance of the hoppers center of mass from its final rest position, k_p and k_s are the respective spring constants of the primary and secondary struts, and s_p and s_s are the strokes (changes in length) of the primary and secondary struts, respectively.

The Lagrangian function is then written as:

$$\mathcal{L} = T^* - V = \frac{1}{2}mv^2 - mgh - \frac{1}{2}k_p^2 s_p^2 - k_s s_s^2 \tag{3}$$

Since two velocity components are given in the customer requirements, at least two generalized coordinates are needed to give an adequate description of the hopper's motion in the worst-case landing scenario. x is defined as the horizontal position of the center of mass and z as its vertical position, with dx and dz as their admissible variations.

The Lagrangian is related to the generalized non-conservative forces Ξ_x and Ξ_z by:

$$\frac{d}{dt}\left(\frac{d\mathcal{L}}{d\dot{x}} + \frac{d\mathcal{L}}{d\dot{z}}\right) - \frac{d\mathcal{L}}{dx} - \frac{d\mathcal{L}}{dz} = \Xi_x + \Xi_z \tag{4}$$

The generalized forces are found from the generalized work done by the dampers:

$$\Xi_x dx + \Xi_z dz = -c_p \dot{s_p} ds_p - 2c_s \dot{s_s} ds_s \tag{5}$$

where c_p and c_s are the respective damping constants of the primary and secondary struts.

4.2 Geometry

Before the equation can be solved, v, h, s_p, and s_s must be expressed in terms of x and z. The height, h, is simply equal to z, and velocity, v, is equal to $\sqrt{\dot{x}^2 + \dot{z}^2}$

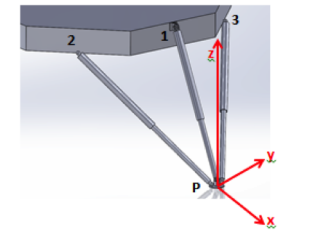

Figure 7: Strut Geometry

Figure 10 shows the geometry of the leg struts. In the figure x_1, y_1,and z_1 are the coordinates of point 1, x_2, y_2, and z_2 are the coordinates of point 2 and so on. The primary strut lies in the xz plane, and the two secondary struts are symmetric about it. If the coordinates of point P, the footpad, are set as zero, the length of the primary strut is:

$$l_p = \sqrt{x_1^2 + y_1^2 + z_1^2} = \sqrt{(x+a)^2 + y_1^2 + (z+b)^2} \tag{6}$$

and the length of each secondary strut it:

$$l_s = \sqrt{x_2^2 + y_2^2 + z_2^2} = \sqrt{(x+c)^2 + y_2^2 + (z+d)^2} \tag{7}$$

where a, b, c, and d are distances from the center of mass.

The un-deformed length of the struts at time $t = 0$, l_{po}, and l_{so} are constants. The strokes of the primary and secondary struts can be expressed as:

$$s_p = l_{p0} - l_p \tag{8}$$

$$s_2 = l_{20} - l_2 \tag{9}$$

With $\dot{s_p}$ and $\dot{s_s}$ equal to $\dot{l_p}$ and $\dot{l_s}$:

$$\dot{s_p} = \frac{(x+a)\dot{x} + (z+b)\dot{z}}{\sqrt{(x+a)^2 + (z+b)^2 + y_1^2}} \tag{10}$$

$$\dot{s_s} = \frac{(x+c)\dot{x} + (z+d)\dot{z}}{\sqrt{(x+c)^2 + (z+d)^2 + y_2^2}} \tag{11}$$

$$ds_p = \frac{(x+a)dx + (z+b)dz}{\sqrt{(x+a)^2 + (z+b)^2 + y_1^2}} \tag{12}$$

$$ds_s = \frac{(x+c)dx + (z+d)dz}{\sqrt{(x+c)^2 + (z+d)^2 + y_2^2}} \tag{13}$$

Substituting (8) and (9) into equation (3) the result is:

$$\mathcal{L} = \frac{1}{2}m(\dot{x}^2+\dot{z}^2) - mgz - \frac{1}{2}k_p(l_{p0}-l_p)^2 - k_s(l_{s0}-l_s)^2 \tag{14}$$

substituting (10) through (13) into (5):

$$\Xi_x dx + \Xi_z dz = -c_p \frac{[(x+a)\dot{x} + (z+b)\dot{z}][(x+a)dx + (z+b)dz]}{(x+a)^2 + (z+b)^2 + y_1^2}$$

$$-2c_s \frac{[(x+c)\dot{x} + (z+d)\dot{z}][(x+c)dx + (z+d)dz]}{(x+c)^2 + (z+d)^2 + y_2^2} \tag{15}$$

$$\Xi_x dx = -c_p \frac{[(x+a)\dot{x} + (z+b)\dot{z}][(x+a)dx]}{(x+a)^2 + (z+b)^2 + y_1^2}$$

$$-2c_s \frac{[(x+c)\dot{x} + (z+d)\dot{z}][(x+c)dx}{(x+c)^2 + (z+d)^2 + y_2^2} \tag{16}$$

$$\Xi_z dz = -c_p \frac{[(x+a)\dot{x} + (z+b)\dot{z}][(z+b)dz]}{(x+a)^2 + (z+b)^2 + y_1^2}$$

$$-2c_s \frac{[(x+c)\dot{x} + (z+d)\dot{z}][(z+d)dz]}{(x+c)^2 + (z+d)^2 + y_2^2} \tag{17}$$

Cancelling dx and dx, the generalized forces are:

$$\Xi_x = -c_p \frac{[(x+a)\dot{x} + (z+b)\dot{z}][(x+a)]}{(x+a)^2 + (z+b)^2 + y_1^2}$$

$$-2c_s \frac{[(x+c)\dot{x} + (z+d)\dot{z}][(x+c)}{(x+c)^2 + (z+d)^2 + y_2^2} \tag{18}$$

$$\Xi_z = -c_p \frac{[(x+a)\dot{x} + (z+b)\dot{z}][(z+b)]}{(x+a)^2 + (z+b)^2 + y_1^2}$$

$$-2c_s \frac{[(x+c)\dot{x} + (z+d)\dot{z}][(z+d)]}{(x+c)^2 + (z+d)^2 + y_2^2} \tag{19}$$

At this point all of the components of the Lagrangian differential equation (4) have been solved for. It can now be evaluated to solve for the equations of motion.

4.3 Governing Differential Equation

Taking the time derivative of the partial derivatives of the Lagrange equation with respect to the horizontal and vertical velocities, $\dot{x}$ and $\dot{z}$ respectively, yields:

$$\frac{d}{dt}\left(\frac{d\mathcal{L}}{d\dot{x}} + \frac{d\mathcal{L}}{d\dot{z}}\right) = m(\ddot{x} + \ddot{z}) \tag{20}$$

Taking the partial derivatives of the Lagrange equation with respect to the horizontal and vertical positions x and z yields:

$$\frac{d\mathcal{L}}{dx} = \frac{k_p(l_{p0} - l_p(z+b)}{l_p} + \frac{2k_s(l_{s0}-l_s)(z+d)}{l_s} \tag{21}$$

and:

$$\frac{d\mathcal{L}}{dx} = \frac{k_p(l_{p0} - l_p(z+b)}{l_p} + \frac{2k_s(l_{s0}-l_s)(z+d)}{l_s} \tag{22}$$

Substituting (18) through (22) into (4):

$$\frac{d}{dt}\left(\frac{d\mathcal{L}}{d\dot{x}} + \frac{d\mathcal{L}}{d\dot{z}}\right) - \frac{\mathcal{L}}{dx} - \frac{\mathcal{L}}{dz} =$$

$$= (\ddot{x}+\ddot{z}) + mg - k_p\left(\frac{l_{p0}}{l_p} - 1\right)(x+z+a+b) - k_s\left(\frac{l_{s0}}{l_s} - 1\right)(x+z+c+d)$$

$$= \Xi_x + \Xi_z \tag{23}$$

$$= -c_p \frac{[(x+a)\dot{x} + (z+b)\dot{z}]}{(x+a)^2 + (z+b)^2 + y_1^2}[(x+a) + (z+b)]$$

$$-2c_s \frac{[(x+c)\dot{x} + (z+d)\dot{z}}{(x+c)^2 + (z+d)^2 + y_2^2}[(x+c) + (z+d)] \tag{24}$$

$$m(\ddot{x} + \ddot{z}) + mg - k_p\left(\frac{l_{p0}}{l_p} - 1\right)(x+z+a+b)$$

$$-k_s\left(\frac{l_{s0}}{l_s} - 1\right)(x+z+c+d)$$

$$= -c_p \frac{[(x+a)\dot{x} + (z+b)\dot{z}]}{(x+a)^2 + (z+b)^2 + y_1^2}[(x+a) + (z+b)]$$

$$-2c_s \frac{[(x+c)\dot{x} + (z+d)\dot{z}}{(x+c)^2 + (z+d)^2 + y_2^2}[(x+c) + (z+d)] \tag{25}$$

In the best-case scenario, the hopper lands perfectly flat and symmetrically on all four legs, and z is the only degree of freedom. All x variations and derivatives then become zero and the governing equation becomes:

$$m\ddot{z} + mg - k_p\left(\frac{l_{p0}}{l_p} - 1\right)(z+b) - 2k_s\left(\frac{l_{s0}}{l_s} - 1\right)(z+d) =$$

$$-\dot{z}\left[c_p \frac{(z+b)^2}{(x_1^2 + (z+b)^2 + y_1^2} + 2c_s \frac{(z+d)^2}{x_1^2 + (z+d)^2 + y_2^2}\right] \tag{26}$$

While there is no analytic solution to either equation (25) or (26), numerical methods are able to approximate the position, velocity, and acceleration as a function of time. With mass, initial position, initial velocity, and geometric constants a, l_{p0}, y_1, etc. specified, the spring and damping constants can be varied to minimize the acceleration experienced.

5 ELECTROMAGNETIC DAMPING THEORY

5.1 Background

A shock absorber is required to attenuate the impact force of the hopper. A shock absorber is a type of mechanical damper that converts kinetic energy into another form of energy that is easily dissipated. It reduces the forces upon a system. The force an ideal damper produces is proportional to an input velocity and is given by:

$$F_d = -cv \tag{27}$$

Where F_d is the damping force, v is the input velocity, and c is a damping constant, determined by the physical parameters of the damper. Upon selecting an electromagnetic damper as the shock absorption solution it became necessary to create a mathematical model that would be able to evaluate an electromagnetic system in the same form as an ideal damper, equation (27).

In order to begin the mathematical model it is important to understand the physical principles that govern the electromagnetic system. The two laws that represent these principles are Faraday's Law and Lenz's Law. Faraday's Law states that any change in the magnetic field of a coil of wire will cause a voltage to be induced. In the situation of a damper, as a magnet passes through the coil the magnetic flux changes, causing a voltage to be induced as seen in Figure 7. The voltage produced is equal to the negative of the rate of change of the magnetic flux multiplied by the number of turns of the coil.

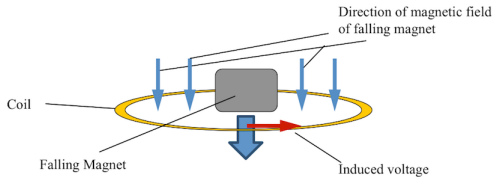

Figure 7: Faraday's Law

Lenz's Law states that any voltage produced by Faraday's Law creates a current. The direction of the current is such that the resultant magnetic field opposes the changing magnetic field that produced it. This opposite magnetic field creates a magnetic braking force, which slows the magnet passing through the coil and is seen in Figure 8.

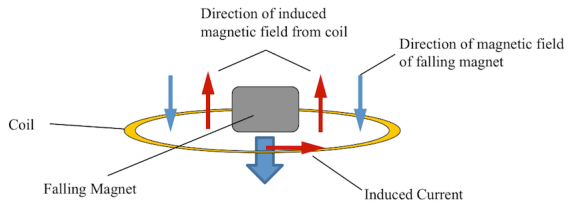

Figure 8: Lenz's Law

After the physical principles had been determined, the mathematical model to express them was developed. Since the electromagnetic damper is a quasi-static system, it is logical to begin the analysis with the quasi-static forms of Maxwell's equations.

The first equation is Lorentzs Law. Lorentzs Law states that a force is experienced by a current passing through a magnetic field. Along a specific direction l parallel to the contour:

$$\vec{F} = \oint i\, d\vec{l}\, x\, \vec{B} \tag{28}$$

Where $\vec{f}$ is the force, i is the current, and $\vec{B}$ is the magnetic field.

Ampere's Law then states that line integral of a magnetic field around a closed contour is equal to the net current passing through the surface of the contour. This equation in integral form is:

$$\oint_c \vec{H} \cdot d\vec{l} = \int_S \vec{J} \cdot d\vec{s} \tag{29}$$

where $\vec{H}$ is the magentic field intensity, $\vec{J}$ is the free current density and $\vec{s}$ is a direction perpendicular to the surface, S.

Faradays Law, mentioned in the preceding section, states that an electric field is generated by a change in magnetic field. It is given in integral form as:

$$\oint_C \vec{E} \cdot d\vec{l} = -\int_S \frac{\partial \vec{B}}{\partial t} \cdot d\vec{s} \tag{30}$$

Where $\vec{E}$ is the electric field. And through a closed space the flux is zero:

$$\oint_C \vec{B} \cdot = 0 \tag{31}$$

There are also two constitutive relations, an electrical and magnetic, to describe a quasi-static system. Ohm's Law gives the electrical relation as:

$$\vec{J} = \sigma \vec{E} \tag{32}$$

Where the free current density, $\vec{J}$, is equal to the electric field multiplied by the material's electrical conductivity, σ.

The magnetic relation is given by:

$$\vec{B} = \mu \vec{H} \tag{33}$$

Where the magnetic flux density, $\vec{B}$ is equal to the permeability of a material, μ, multiplied by the magnetic field intensity, $\vec{H}$. For non-ferromagnetic materials $\mu \approx \mu_0$ where μ_0 is the permeability of free space. For ferromagnetic materials, μ is approximated as $\mu = \mu_0 \mu_r$ where μ_r is the relative permeability of the material. It is important to note that

μ is a function of $\vec{H}$ and is not constant. The relationship between the magnetic flux density and the field intensity is usually represented by a hysteresis loop. The remanent flux density and the coercive force, are used to approximate the demagnetization curve:

$$B_m = B_{rem} + \mu_{rec} H_m \tag{34}$$

where B_m is the flux density, B_{rem} is the remanent flux density, H_m is the field intensity, and μ_{rec} is the recoil permeability which is given by the remanent flux density divided by the coercive force. The operating point of the magnet is then given as (B_m,H_m) which fluctuates along the hysteresis loop according to the properties of the electromagnetic system.

5.2 Electromagnetic Mathematical Model

A simplified representation of the electromagnetic damper was then used to develop the mathematical model. It can be seen in Figure 9. After selecting the configuration, the characteristics of the damper were determined.

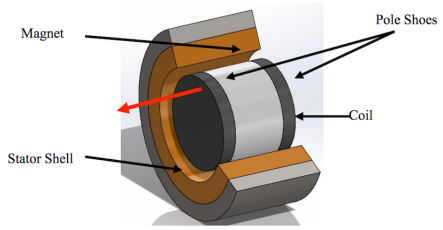

Figure 9: Damper Cross Section

The characteristics of the damper are as follows:

- There is a short mover inside of the stator.
- The mover consists of a single cylindrical permanent magnet that is axially magnetized between two ferromagnetic pole shoes.
- The stator is ferromagnetic and the coil has a single winding phase.
- The length of the coil equals the length of the mover.
- The stroke of the damper (for the purpose of this analysis) is the length of the magnet

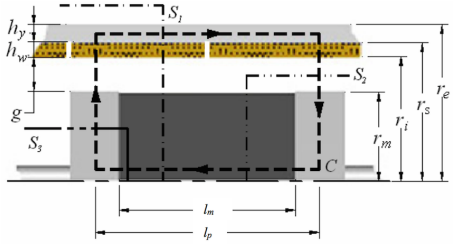

Figure 10: Damper Cross Section

A diagram of the parameters is shown in Figure 10 and they are then listed and defined in Table 1.

Table 1: Damper Parameters

Name	Symbol	Description
Pole Pitch	l_p	Distance between adjacent poles or radial magnets
Magnet Length	l_m	Length of magnets
Pole Shoe Width	l_f	Width of the pole shoes
Air Gap Thickness	g	Distance between mover and coil
Number of Poles	p	Number of poles in the damper
Coil Height	h_w	Height of coil
Coil Width	l_w	Width of coil
Wire Radius	r_w	Radius of the coil's wire
Coil Turns	N_w	Number of turns on each coil
Active Coil Turns	N_a	Number of turns on the coil intercepted by the pole shoe flux
Mover Radius	r_m	Radius to the outside of the magnets or the pole pieces
Armature Radius	r_i	Radius to the inside surface of the armature
Stator Radius	r_s	Radius to the inside surface of the stator or ferromagnetic shell
Machine Radius	r_e	Radius to the outside surface of the damper
Stator thickness	h_y	Thickness of the armature shell

Based upon the above damper configuration and the derivation in [3] the relation between the magnet's flux density, found from Apere's Law and H_m y is given as:

$$B_m = \frac{B_{rem}\, l_m\, l_f}{l_m\, l_f + r_m^2 \frac{\mu_{rec}}{\mu_0} \left(ln\left[\frac{r_s}{r_m}\right] + \frac{1}{2\mu_S} + \frac{l_p\, l_f}{\mu_S\, h_S\, (r_s + r_e)} \right)} \tag{35}$$

To then find the force upon the mover due to the induced current in the coil, Lorentz's Law (20) is used. This current produces a magnetic field that opposes the mover's magnetic field according to Lenz's Law. The force is expressed as:

$$F_d = pN_a \oint i\, d\vec{l} \times \vec{B_C} \tag{36}$$

where p is the number of magnets, N_a is the number of loops in the coil intercepted by the flux, d$\vec{l}$ is the direction of the coil and $\vec{B_c}$ is the magnetic field in the coil. Substituting $\vec{B}$ from [3]:

$$F_d = pN_a(2\pi\, r\, i)\frac{r_m^2}{2l_f\, r} B_m = \pi\, pN_a \frac{r_m^2}{l_f} B_m\, i \tag{37}$$

$$\pi\, p\, N_a \frac{r_m^2}{l_f} B_m = K_t \tag{38}$$

where K_t is known as the "machine constant" and has units of [N/A][3].
Faraday's Law can now be used to evaluate the voltage-velocity relationship of the coil and the mover. This relationship is given as:

$$V = \pi\, p\, N_a \frac{r_m^2}{l_f} b_m\, v = K_t\, v \tag{39}$$

The induced voltage is related to the velocity by the same machine constant from the Lorentz force. Using the equation for B_m (35), K_t can be found as:

$$K_t = \frac{\pi r_m^2 B_{rem} l_m l_f p N_a}{l_m l_f + r_m^2 \frac{\mu_{rec}}{\mu_0}\left(ln\left[\frac{r_s}{r_m}\right] + \frac{1}{2\mu_S} + \frac{l_p l_f}{\mu_S h_S (r_s + r_e)}\right)} \tag{40}$$

From this, it can be deduced that K_t and the circuit parameters determine the force-velocity relationship of the damper[3].

Now, using the force velocity relationship and the resistance-inductance relationship from [3], the damper can be modeled using an ideal transformer relationship with the form of:

$$\begin{cases} e = K_t\, v \\ F_d = K_t\, i \end{cases} \tag{41}$$

Using the transformer relationship the force-velocity relationship becomes:

$$L_{coil}\frac{dF_d}{dt} + R_{coil}\, F_d = K_t^2\, v \tag{42}$$

This first order differenctial equation can beput in the form of:

$$\tau\frac{d\nu}{dt} + \nu = F(t) \tag{43}$$

$$\frac{L_{coil}}{R_{coil}}\frac{dF_d}{dt} + F_d = \frac{K_t^2\, v}{R_{coil}} \tag{44}$$

Dropping the magnet applies an instantaneous velocity to the system. This input can be described by the step function:

$$F(T) = \begin{cases} t < 0,\ 0 \\ t \geq 0,\ \frac{K_t^2\, v}{R_{coil}} \end{cases} \tag{45}$$

Now plugging in (45) to (44):

$$\frac{L_{coil}}{R_{coil}}\frac{\overset{0}{\cancel{dF_d}}}{\cancel{dt}} + F_d = \frac{K_t^2\, v}{R_{coil}} \tag{46}$$

$$F_d = \frac{K_t^2\, v}{R_c oil} \tag{47}$$

This can now be recognized as the ideal damper equation (27) with the damping coefficient equal to the machine constant squared over the coil resistance:

$$c_d = \frac{K_t^2}{R_{coil}} \tag{48}$$

Now that the parametes that determine the damping coefficient and the operation point of the magnet were solved for, the electromagnetic dampers for a prototype and the final landing gear could be designed.

6 PROTOTYPE DESIGN, CONSTRUCTION, AND TESTING

6.1 Design

To test the functional relationship between the parameters of the damper and the damping force achievable, a physical prototype of a single strut was constructed and vertical drop tests on it were performed, in order to determine the damping constant to compare to a calculated theoretical value.

Table 2: Prototype Design Parameters

Parameter	Model Value	Determines	Determines	Determines
Stroke/coil length	0.19 m	Travel distance (+)		Velocity at impact (-)
Wire diameter	0.00145 m	Resistance (+)	Damping constant (-)	Deceleration (+) Maximum load (+) Velocity at impact (-)
Number of coil layers	5	Resistance (-)		
Magnet width	0.0254 m	Resistance (+)	Damping constant (+)	
Magnet radius	0.0254 m	Machine constant (+)		
Number of magnets	2			
Air gap width	0.0011 m	Machine constant (-)		
Pole shoe width	0.00635 m			
Spring constant	145.355 N/m			Deceleration (-) Maximum load (-) Velocity at impact (+)

Table 2 shows the theoretical relationship between the design parameters and the resulting characteristics of the damper, derived from the equations in the preceding section and assuming a magnet grade of N42. The first column lists independent variables. The second shows the value of each parameter in the prototype. The subsequent columns list the dependent variables, with signs in parentheses indicating a positive or negative correlation with the preceding variable. For instance, increasing the number of coil layers increases the coil resistance, and increasing the resistance decreases the damping constant. However, adding more layers also increases the value of the machine constant, which has a positive correlation with the damping constant.

The design of the prototype began by simplifying the landing gear to a single strut. The neodymium magnet grade and radius, based on existing sinusoidal dampers, were chosen to fit the required damping density. The electromagnetic mathematical model was used to determine the other necessary components such as the radius of copper wire, the air gap, and the size of the pole shoes needed to direct the magnetic flux. The prototype consisted of a mover, with two shafts, two pole shoes and a magnet. The pole shoes and magnet were radially constrained. The stator contained the coils, bearings to concentrically constrain the mover, and the spring to reset the damper. The design can be seen in Figures 11 and 12. The aim of the prototype was

to maximize the dynamic load that the device could support while keeping the acceleration under 10 Earth gs (98 m/s^2), the peak deceleration recorded by the most recent Mars lander[4]. The velocity at impact (i.e. the final velocity, just before the shaft contacts the inside of the cylinder) was to be kept to a minimum.

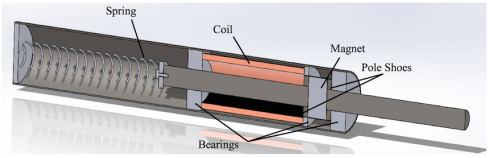

Figure 11: Prototype Cross Section

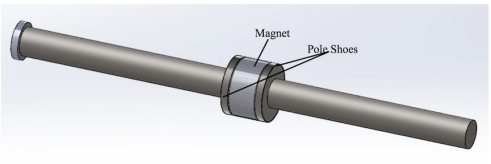

Figure 12: Mover Assembly

6.2 Construction

The construction of the prototype began by wrapping the copper wire into a single long coil. This was accomplished using a lathe and hand wrapping the copper wire tight around a plastic tube. After some preliminary testing it was found that the single long coil did not function well, as the induced voltage in the coil is constant. This also made the current, and thereby the induced magnetic field, constant across the length of the coil. The magnet, however, only interacts with fields in its immediate vicinity. To increase the current density and the force on the magnet, the single coil was replaced by an array of smaller coils totaling the same length. The same wrapping procedure was done for six coils with their lengths being equal to the width of the magnet, 2.54cm. Each coil had five layers, each separated by a layer of electrical tape, seen in Figure 13.

Figure 13: Coil Array

The bearings used to constrain the mover and coil were turned on a lathe to the proper length, inner radii, and outer radii. The bearings were press-fit into the stator tube using a lathe's tailstock barrel. The end cap was machined from a cylinder of aluminum. Half of the cylinder was turned until it matched the inner diameter of the stator tube. Three tapped holes were drilled into the end cap and outer housing so that the it could be secured with screws.

Three pole shoes were turned from a steel rod into discs of diameters equal to those of the magnets. The two outer pole shoes have a hole in the center with a diameter equal to that of the mover shafts. The steel rod was cut in half using a chop saw and each half was inserted into the pole shoe holes, using the magnetic attraction to secure the shaft. Two mover assemblies were created, one with a single magnet and one with two magnets. The entire prototype was then assembled as seen in Figures 14 through 16.

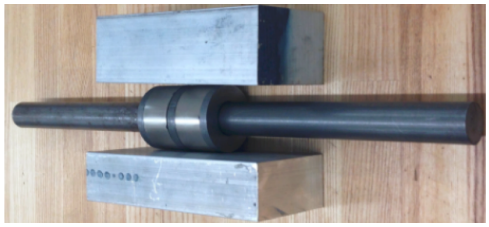

Figure 14: Prototype Mover

Figure 15: Prototype Stator (Exploded)

Figure 16: Completed Prototype

6.3 Testing

To determine the accuracy of the mathematical model, the damping constnt of the prototype was found through an experimentally determined equation of motion. The form of the equation was first derived with the damping constants and integration constants undetermined. Then drop tests were performed and position vs. time data recorded for

each. Fitting the equation to each data set yielded experimental values for the damping constant.

The device is modeled as a mass falling under the influence of gravity with a damper. The system has one degree of freedom, the distance v from the ground to the cylinder. The potential energy V and kinetic energy T of the system are:

$$V = mgz \tag{49}$$

$$T = \frac{1}{2}m\dot{z}^2 \tag{50}$$

where m is the total mass of the stator and all hardware attached to it and g is the gravitational constant of 9.8 m/s^2. The Lagrangian function is then:

$$\mathcal{L} = T - V = m\left(\frac{1}{2}\dot{z}^2 - gz\right) \tag{51}$$

The generalized work done by the damper is given as $\Xi = -c\dot{z}$, where c is the damping constant. The generalized work is related to the Lagrangian by the following equation:

$$\frac{d}{dt}\frac{d\mathcal{L}}{d\dot{z}} - \frac{d\mathcal{L}}{dz} = \Xi \tag{52}$$

Substituting (51) into (52) yields:

$$m\ddot{z} + gm = c\dot{z} \tag{53}$$

The solution to this differential equation takes the form of:

$$z(t) = -\frac{gm}{c}t + \frac{k_1 m}{c}e^{-\frac{c}{m}t} + k_2 \tag{54}$$

Where k_1 and k_2 are constants of integration.

After determining the governing equation the experiment was performed. The spring was removed from the prototype. With the mover fully extended, the prototype was dropped mover first from a height of 0.31m between the end of the shaft and the floor. A test stand constrained its motion with a vertical tube during the fall. During the initial 0.31m drop the motion was undamped freefall. Damped motion began when the shaft first hits the ground, at which time the velocity of the stator was 2.5 m/s

Table 3: Equipment List

Instrument	Make	Model
Optical sensor	Sick	WTA24-P5401
Power supply	Hewlett Packard	E3631A
DAQ board	National Instruments	BNC-2090
Scale	Ohaus	Brainweigh B5000

To calibrate the sensor, listed in Table 3, it was connected to the power supply and data acquisition board. It was clamped to a table and two meter sticks were clamped to the edge of the same table to serve as a length scale. Once the sensor was active and recording voltage vs. time data in LabVIEW, a white sheet of paper taped to a block was moved along the scale in 0.05m increments and the mean voltage at each increment recorded.

The sensor was then mounted over the prototype using an adjustable stand on top of a table. For better reflectivity and thereby more accurate measurements, a piece of white paper was attached to the cap of the stator tube.

The sensor had an operating range of 0.6 to 1.2m, so it was positioned in a manner that the maximum and minimum heights of the reflecting surface fell within that range. The LabVIEW Virtual Instrument was set to record voltage for three seconds at 150 samples per second. The prototype was raised to 0.31m, the program recording initiated, and the prototype was dropped. This test was repeated five times. A second magnet was added to the mover and five more tests were performed in the same manner. Finally, the device was held steady at the initial impact height (where the shaft first touches the ground) and the mean voltage was recorded. This value marked the transition from freefall to damped motion. Figures 17 and 18 show a representative plot of the useful position vs time data obtained from tests of each magnet configuration

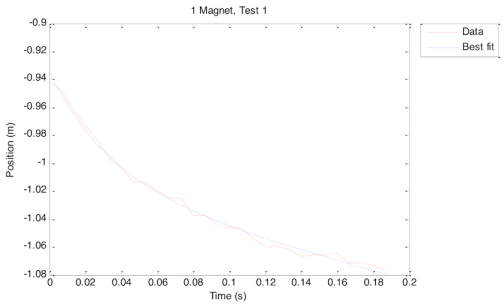

Figure 17: Damped Motion for Single Magnet

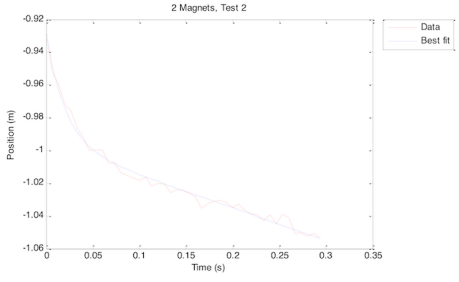

Figure 18: Damped Motion for Double Magnet

A calibration function was calculated from the curve fit in Figure 18. The function was:

$$x = 0.192\,V + 0.897 \tag{55}$$

where V is voltage (in volts) and x is position (in meters). This function is applied to all data sets to obtain position vs. time.

Using the initial impact height and the final position, the data ranges that represent only the damped motion of the device are graphically selected from each set. MATLAB was used to fit equation **(X)** to the selected position and time ranges from each test and return the damping constant c. The average c from all five trials was computed for both magnet configurations. Following this, an uncertainty analysis was performed and the resultant experimental values for the damping constants were calculated as:

$$\sigma_{c_{1mag}} = 91.1 \pm 8.8 \, \frac{N \cdot s}{m}$$

$$\sigma_{c_{2mag}} = 176 \pm 14 \, \frac{N \cdot s}{m}$$

From the above data, when compared to the theoretical damping constants, as predicted by the mathematical model below, it can be seen that the tests of the prototype confirmed the validity of the mathematical model.

$$\sigma_{c_{1mag}} = 91.3 \, \frac{N \cdot s}{m}$$

$$\sigma_{c_{2mag}} = 183 \, \frac{N \cdot s}{m}$$

7 FINAL DESIGN

7.1 Simulation

In order to begin the final design, it was necessary to calculate the landing forces upon the hopper. From these landing forces the physical parameters of the landing gear could be created. As stated in the Landing Dynamics section earlier, the equations of motion for the vehicle (equations (25) and (26)) were not analytically solvable. The system has twelve damper-spring pairs and up to four degrees of freedom and was modeled with a SolidWorks Motion Study simulation.

The limits of the system were then established. First, the maximum allowable acceleration was determined. There is no standard acceleration limit for electronic components on planetary landers. The peak deceleration of the Mars Phoenix lander[4] was 9.2 Earth g (90.16 m/s^2). However, the customer suggested the acceleration rating for ordinary commercial electronics of 40 Earth g, or 392 m/s^2 as a baseline. According the hopper designers, all the components on the hopper will be, quite robust for earth launch, so a value of 392 m/s^2 was accepted as the threshold.

The dimensions of the legs were then determined based on the limited information available on the potential hopper dimensions and landing conditions. Given the leg span of 4 meters and body span of 1.5 meters, each leg must extend 0.75m horizontally from the edge of the body. Although no minimum ground clearance was specified, the maximum obstacle diameter of 0.5m provided a convenient substitute. The initial ground clearance was set to 1.5m.

7.2 Worst-Case Scenario

To simulate the maximum force that a leg would have to bear (maximum vertical and horizontal velocity into a 20-degree slope on one leg), an assembly was created consisting of all four legs, with footpads, attached to an octagonal body representing the body of the hopper. Primary struts were attached to the body and footpads with hinges, and secondary struts were attached with ball joints. Each strut was modeled in two telescoping segments, with a damped spring element added in between them. An aluminum-to-steel solid body contact condition was also set between the two segments.

The hopper assembly was positioned above a solid body with a 20-degree slope, to which one footpad was fixed (assuming that the first leg to touch down hits an obstacle and does not move). The mass of the hopper body was set to 1000 kg and its initial velocity to 2m/s horizontal (toward the slope) and -2.5 m/s vertical, seen in Figure 2. A solid body contact condition was set between the other footpads and the slope, with relatively high friction. The three free legs were constrained to maintain their position relative to the body until just before they touched down. Gravity was set to 3.73 m/s^2, the gravitational acceleration on Mars.

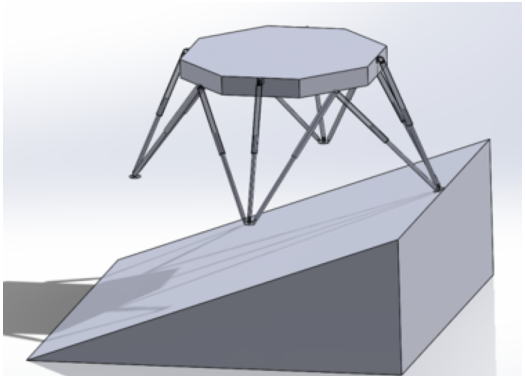

Figure 19: Worst-Case Initial Position

The motion study was set to record the magnitudes of the body's velocity and acceleration. The acceleration caused by the first leg to touch down is of most concern, since that leg bears the highest force. Figure 19 shows the initial position of the hopper and Figure 28 shows the position shortly after all four legs have touched down.

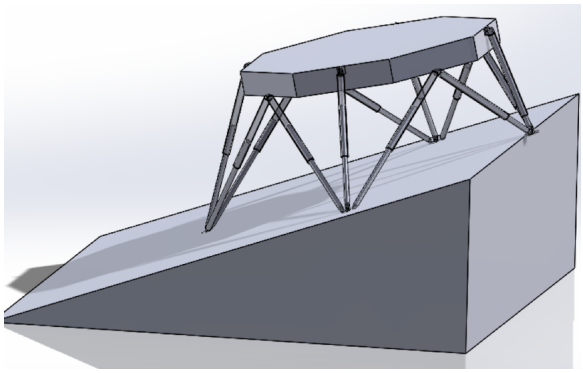

Figure 20: Worst-Case Final Position

The simulation was run repeatedly, adjusting the damping and spring coefficients each time to improve the acceleration. In a more symmetrical landing, the maximum acceleration would be expected at the initial touchdown of the footpads. However, the hopper undergoes a large rotation between the touchdown of the foremost leg and that of the other legs. This means that the struts of this leg compress nearly their full stroke before any of the others begin to bear any force. Figure 21 gives the velocity and acceleration data recorded by the study with all spring constants set to 800 N/m and all damping constants set to 1000 N s/m.

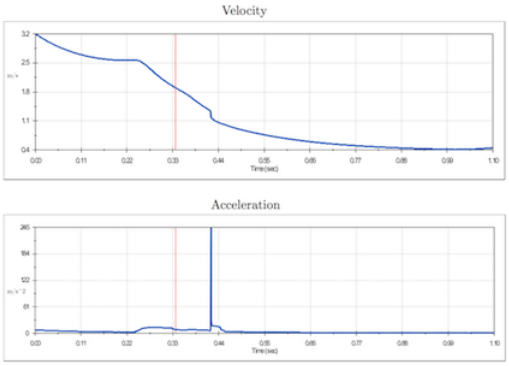

Figure 21: Simulated v and a Results (Worst-Case)

Of interest is the region up to and including the acceleration peak of 244.74 m/s^2 at 0.422 s. This occurs when the primary strut of the foremost leg is fully compressed and its two segments come into contact. The significance of this peak is questionable, since it only affects a portion of the hopper and the presence of a spring would change the characteristics of the actual impact. Assuming the acceleration really reaches this maximum, however, it still falls below the customer's threshold of 392 m/s^2.

7.3 Best-Case Scenario

Although the landing gear is designed for the worst-case scenario, it is also useful to consider the best-case scenario (no horizontal velocity, symmetrical landing onto a perfectly flat surface seen in Figure 8). In this case, all twelve dampers are active from the start, so if the damping constant is set too high for the sake of the worst-case landing, the initial acceleration could be undesirably high.

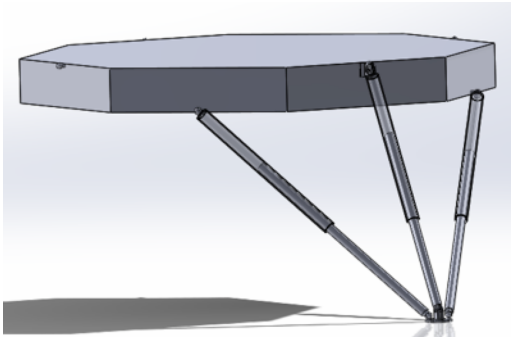

Figure 22: Best-Case Scenario Setup

The best-case scenario is comparatively simple to model, being symmetrical and having only one degree of freedom. Once the mass of the body is set to 250 kg, a quarter of its actual mass, only one leg is necessary (shown in Figure 22) for simulation purposes. The body is constrained to move only in the vertical direction, and its initial velocity is set to -2.5 m/s.

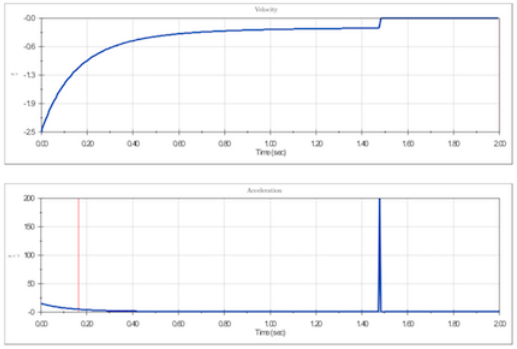

Figure 23: Simulated v and a Results (Best-Case)

The velocity and acceleration recorded from this simulation are displayed in Figure 23. As before, the peak in acceleration indicates the moment of contact between the two segments of the primary strut. Based upon the results of these simulations the final values of the design parameters can be seen in Table 4.

Table 4: Design Values Selected from Motion Study

Primary strut stroke	**0.667 m**
Secondary strut stroke	0.600 m
Primary strut damping constant	1000 N s/m
Secondary strut damping constant	1000 N s/m
Primary strut spring constant	800 N/m
Secondary strut spring constant	800 N/m

7.4 Landing Gear Design

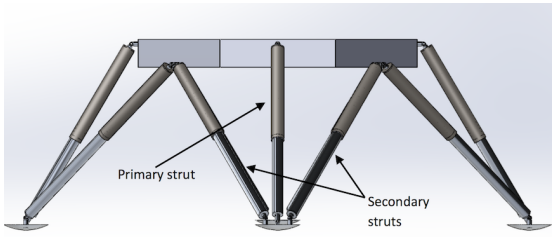

Figure 23: Final Landing Gear Design

The final strut design seen in Figure 23 differs most notably from the prototype design in that the separator tube between the magnets and coils, originally intended to be part of the mover and encase the magnets, is now part of the stator and runs the entire length of the coil array (see Figure 26). It will be made of Teflon and provide a smooth sliding surface for the magnets. The mover will thus be constrained by one linear bearing and the separator tube, eliminating the need for a second shaft and bearing and effectively halving the length of the stator tube.

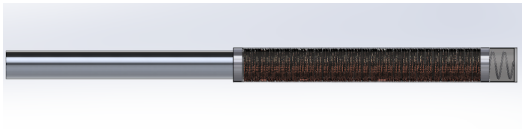

Figure 24: Primary Strut Internal View

The shaft from the prototype will be replaced by an aluminum tube. One of the pole shoes will be machined to fit inside this tube as shown in figures 26 and 27, and secured with space-qualified epoxy. Epoxy will also be applied to the rest of the magnets and pole shoes to keep them aligned. The bearing, a composite dry plain bearing from SKF, will be press fit into the tube inside a supporting ring. Another ring will be press fit behind the coils to hold them in place. A centimeter-thick end cap will be welded onto the free end of each tube. The space between the end of the coil array and the end cap, as seen in Figures 24 and 26, will be occupied by the spring when it is fully compressed. The springs will be custom ordered from WB Jones. As in the prototype, the magnets are grade N42 NdFeB and axially magnetized, the wire gauge is 16, and the orientation of each coil is irrelevant.

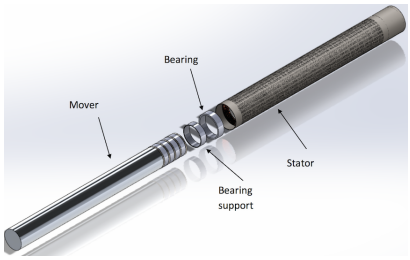

Figure 25: Primary Strut Exploded View

Although other landing configurations are possible, these struts are designed to be attached to the Mars hopper in an inverted tripod configuration, as shown in Figure 23. The primary struts can be attached to the body and footpads using hinge joints, while the secondary struts should be attached with ball or universal joints to eliminate bending moments. Table 5 lists the values of the relevant design parameters. All except the dimensions of the spring and mover tube affect the damping performance in some way and can be modified using the mathematical model and simulation methods previously described if different characteristics are desired.

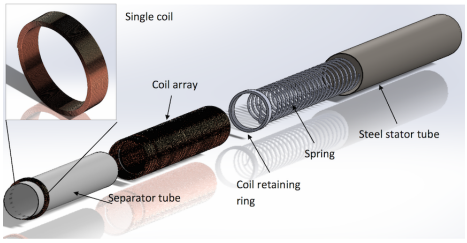

Figure 26: Exploded View of Stator

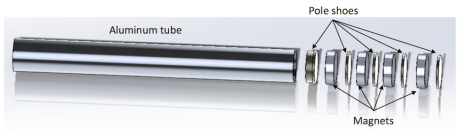

Figure 27: Exploded View of Mover

Table 5: Final Design Parameters

Parameter	Final Value
Magnet radius	0.0484 m
Magnet width	0.0254 m
Remanent flux density	1.32 T
Number of magnets in primary strut	4
Number of magnets in secondary strut	4
Wire diameter	0.00146 m
Coil width	0.0254 m
Number of layers per coil	5
Number of coils in primary strut	30
Number of coils in secondary strut	29
Pole shoe width	0.00635 m
Pole shoe radius	0.0484 m
Stroke of primary strut	0.667 m
Stroke of secondary strut	0.6 m
Spring constant of primary strut	800 N/m
Spring constant of secondary strut	800 N/m
Spring diameter	0.096 m
Outer radius of stator tubes	0.0582 m
Thickness of stator tubes	0.00165 m
Outer radius of mover tubes	0.0475 m
Thickness of mover tubes	0.005 m
Thickness of separator tubes	0.001 m

8 DESIGN EVALUATIONS

In order to gauge the degree of success achieved for the design it must be evaluated. The prototype, mathematical models, and the final landing gear design are all necessary for this analysis. The prototype was designed and fabricated to test the predictions of the electromagnetic damper mathematical model. It was designed around the grade and sizes of magnets available in the project budget. A more practical design approach for an unlimited budget would have been to design the leg and select the magnets and damper components necessary to achieve desired values for the damping constant and peak acceleration. However, this proved unnecessary, as the prototype performed its role in determining the damping constant for the damper.

The next design aspects necessary to were the mathematical models. The mathematical models included the landing dynamics and electromagnetic damper models. The landing dynamics model was solved through numerical methods. In retrospect, now knowing that the equations derived were analytically unsolvable, it would have been more practical to approach the problem from a simulated standpoint initially. Simulation then provided the insight needed to make all of the final design decisions. The electromagnetic model was developed to calculate the parameters of the damper to attenuate the impact. It was proven to be an accurate model through the testing of the prototype. The dynamics simulation sequence and the electromagnetic mathematical model also had an additional benefit. They could be used in conjunction to calculate the dynamic forces, damping requirements, and damper design for any future landing vehicles with a similar design.

The final design of the landing gear was the purpose of the entire project. By using the prototype and the mathematical models the parameters of the design were chosen and modeled. Upon the completion of the design it was simulated to test if it could withstand the forces it would be subjected to during an actual Mars landing. This simulation proved that the landing gear design could support far more than the required forces.

8.1 Financial Analysis

The total cost of the single strut prototype was about $260. It was found that the Neodymium magnets and the copper wire were the most expensive parts of the system. The wire accounted for roughly 26% percent of the total cost and the magnets accounted for approximately 36% of the total cost. To estimate the total cost of the final design, the price per kilogram of each material in it was multiplied by its density and volume. This yields the price of each material by the mass required for the design. This was calculated for the steel, aluminum, and copper wire. These values were added together and 15% of this value was added in to factor the cost of springs, bearings and manufacturing costs.

$$Cost = \left(m \cdot \frac{Price}{kg}\right)_{Cu} + \left(m \cdot \frac{Price}{kg}\right)_{Al} + \left(m \cdot \frac{Price}{kg}\right)_{steel} + \left(N_{mags} \cdot \frac{Price}{(N_{mags} = 1)}\right) + .15(\sum Cost_{Cu,Al,St,Mag})$$

$$= (134\,kg \cdot 6.77\,\$/kg)_{Cu} + (25\,kg \cdot 1.76\,\$/kg)_{Al}$$

$$(96\,kg \cdot 1.10\,\$/kg)_{Steel} + (48mag \cdot 228\$/mag)$$

$$+.15(\sum Cost_{Cu,Al,St,Mag})$$

$$Cost \approx \$13,800$$

This gave an estimated final design cost of $13,800. To put this seemingly high cost into perspective, the NASA Mars Opportunity rover and Phoenix lander had a total mission cost of $400 million and $386 million respectively. A significant portion of the cost of those vehicles was dedicated to the landing system, as it is one of the most essential systems for the mission to succeed. The final price of the electromagnetic landing gear design represents only a fraction of the cost of a typical Mars mission and therefore is a financially feasible solution.

9 CURRENT STATUS AND FUTURE STEPS

At the present time, the prototype has been tested in a single magnet and dual magnet arrangement. Based upon the results of those tests the final design of the landing gear was generated.

There are several steps required to implement this landing gear design into the actual Mars Hopper. The first step is to take the results of the prototype testing and use them to refine the electromagnetic damper mathematical model. Upon the adjustment to the mathematical model, larger scale testing would need to be done. A single leg with three struts and a scale model of the entire hopper should be tested. If the testing is successful, the landing gear design could then be completed, including the design of internal and external components to allow for operation on the surface of Mars. After the landing gear design is completed it needs to be integrated into the Mars hopper's design. This would be done through joints that connect the landing gear to the footpads and to the hopper body.

10 CONCLUSIONS

The University of Leicester Mars hopper requires a resettable landing gear design. An electromagnetic landing gear is an effective solution for this issue. The final design of the electromagnetic landing gear can withstand forces greater than that experienced by the hopper during landing. The mathematical model governing the electromagnetic shock absorber and landing dynamics simulations can also be used to create different configurations of the landing gear based upon the desired landing conditions.

11 Works Cited

[1] Williams, H.R., Ambrosi, R.M., and Bannister, N.P. "A Mars hopping vehicle propelled by a radioisotope thermal rocket: thermofluid design and materials selection". Proceedings of the Royal Society A, 17 November 2010.

[2] Zupp, George A. and Doirion, Harold H. "A mathematical procedure for predicting the touchdown dynamics of a soft-landing vehicle". Washington, D.C: National Aeronautics and Space Administration, 1971.

[3] Palomera-Arias, Rogelio. "Passive Electromagnetic Damping Device for Motion Control of Building Structures". Massachusetts Institute of Technology, 2005.

[4] Desai, Prasun N., Prince, Jill L., Queen, Eric M., and Cruz, Juan R. "Entry, Descent, and Landing Performance of the Mars Phoenix Lander." AIAA, 2008.